Optical Engineering

OpticalEngineering.SPIEDigitalLibrary.org

Swing arm profilometer: analytical solutions of misalignment errors for testing axisymmetric optics

Ling Xiong
Xiao Luo
Zhenyu Liu
Xiaokun Wang
Haixiang Hu
Feng Zhang
Ligong Zheng
Xuejun Zhang

Ling Xiong, Xiao Luo, Zhenyu Liu, Xiaokun Wang, Haixiang Hu, Feng Zhang, Ligong Zheng, Xuejun Zhang, "Swing arm profilometer: analytical solutions of misalignment errors for testing axisymmetric optics," *Opt. Eng.* **55**(7), 074108 (2016), doi: 10.1117/1.OE.55.7.074108.

Optical Engineering 55(7), 074108 (July 2016)

Swing arm profilometer: analytical solutions of misalignment errors for testing axisymmetric optics

Ling Xiong,[a,b,*] Xiao Luo,[a] Zhenyu Liu,[a] Xiaokun Wang,[a] Haixiang Hu,[a,b] Feng Zhang,[a] Ligong Zheng,[a] and Xuejun Zhang[a]
[a]Changchun Institute of Optics, Key Laboratory of Optical System Advanced Manufacturing Technology, Fine Mechanics and Physics, Chinese Academy of Sciences, No. 3888 Dong Nanhu Road, Changchun, Jilin 130033, China
[b]University of Chinese Academy of Sciences, Beijing 100049, China

Abstract. The swing arm profilometer (SAP) has been playing a very important role in testing large aspheric optics. As one of most significant error sources that affects the test accuracy, misalignment error leads to low-order errors such as aspherical aberrations and coma apart from power. In order to analyze the effect of misalignment errors, the relation between alignment parameters and test results of axisymmetric optics is presented. Analytical solutions of SAP system errors from tested mirror misalignment, arm length L deviation, tilt-angle θ deviation, air-table spin error, and air-table misalignment are derived, respectively; and misalignment tolerance is given to guide surface measurement. In addition, experiments on a 2-m diameter parabolic mirror are demonstrated to verify the model; according to the error budget, we achieve the SAP test for low-order errors except power with accuracy of 0.1 μm root-mean-square. [DOI: 10.1117/1.OE.55.7.074108]

Keywords: optic testing; profilometer; alignment; aspherics.

Paper 160811 received May 24, 2016; accepted for publication Jun. 30, 2016; published online Jul. 20, 2016.

1 Introduction

The swing arm profilometer (SAP) was first reported by Anderson et al.[1,2] in the 1990s. The testing theory of the SAP is based on the fact that all measuring instruments have an accuracy that is proportional to their total range; to test an aspheric surface, the minimum testing range is the departure from its best-fit sphere. The way to achieve this is to move the sensor along the vertex sphere. Based on the geometry of a sphere generator, SAP was implemented with a sensor attached to the end of a radius rod pivoting to the center of the sphere. It is useful and highly efficient for large mirrors exceeding the range of a coordinate-measuring machine.

The SAP test has been playing a very important role in testing large aspheric optics. As the pioneer of the SAP test, the Arizona group has reported outstanding results for measuring large optics;[1–7] Compared with the interferometer null test with the 43 low-order Zernike terms removed, the accuracy of SAP for testing 1.4-m mirror is 5 nm in root-mean-square (RMS). Groups from London and Chengdu China have also done excellent work on SAP testing, achieving SAP testing for a 350-mm diameter mirror within uncertainty of 0.16 μm in peak-valley (PV) and 0.02 μm in RMS[8–11] without low-order terms removed. The accuracy of other works from South Korea[12] or Changsha China[13] was reported to be microns in PV. Changchun Institute of Optics, Fine Mechanics, and Physics has achieved success in measuring an aspheric mirror up to 2 m in diameter by SAP with an accuracy of ~2 μm in PV without low-order terms removed except power.[14]

For improving the test accuracy, the important guarantee is supposed to be alignment and calibration.[5,6,15] An ideal SAP test is to align SAP in a position related to the mirror under test and assure the trajectory of the sensor probe on best-fit sphere (BFS) of optic, while in fact, SAP cannot be aligned in a perfect way due to alignment error. It turns out that alignment error is an important error source that leads to low-order errors such as aspherical aberrations, astigmatism, and coma apart from power. SAP is used to measure optic surface during the grinding process,[7,11,15–17] when surface accuracy comes to 1 to 2 μm in PV; the effect of misalignment except for power comes to show up and cannot be ignored.

In this paper, we present how misalignment of SAP components impact on tests of axisymmetric optical. The analysis has been applied for a 2-m diameter parabolic surface. Model setup and analysis are presented in Sec. 2 as follows. Basic principle of SAP is first described in Sec. 2.1. An analytical model is built as relation between axisymmetric surface and alignment parameters of SAP given in Sec. 2.2. Then by performing partial derivative and series expansion, the solutions of errors that misalignment elements produced on surface test result are derived in Sec. 2.3. Based on the solutions, misalignment tolerance for the SAP test of 2-m mirror is proposed in Sec. 2.4. Experiment and verification are reported in Sec. 3. The verification of the analytical model is presented with experiment on a misalignment parameter in Sec. 3.1. The verification of SAP test compared with interferometer test is presented in Sec. 3.2. The conclusion is given in Sec. 4.

The paper is aimed to present the preparatory work for decoupling misalignment errors from test results in low-order terms. Further analysis of misalignment errors for testing off-axis aspheric optics are in process.

*Address all correspondence to: Ling Xiong, E-mail: xyznpp@126.com

0091-3286/2016/$25.00 © 2016 SPIE

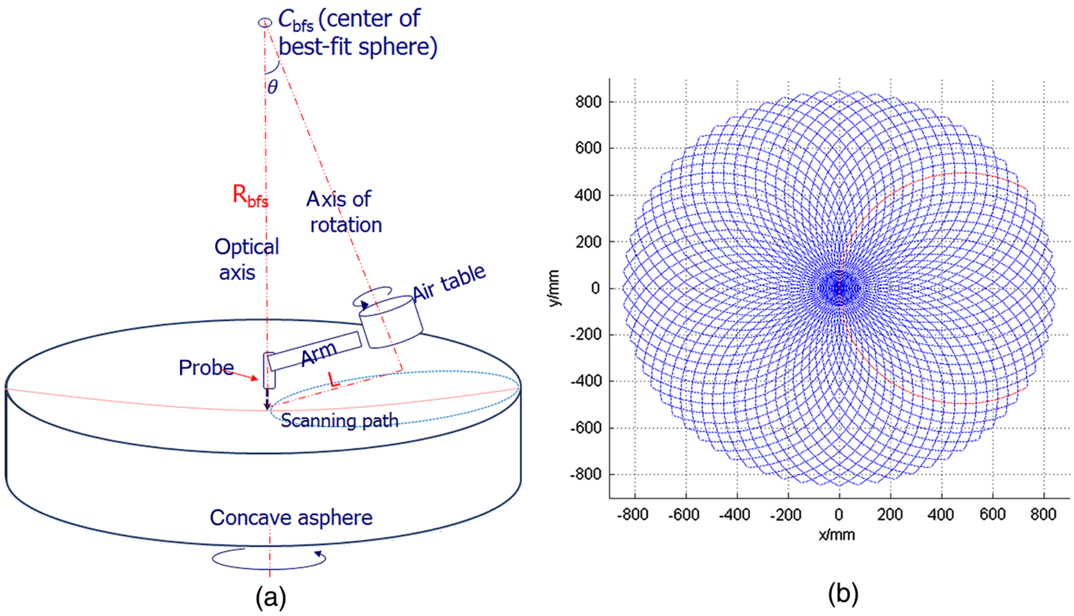

Fig. 1 Basic principle of SAP test: (a) geometry of SAP and (b) scan pattern.

2 Model and Analysis

2.1 *Basic Principle of Swing Arm Profilometer*

The basic geometry of the SAP[1–3] is shown in Fig. 1(a). A probe is mounted at the end of an arm that is fixed on a high accuracy air-table whose rotation axis is tilted and goes through the center of BFS. By rotating the mirror, two-dimensional profile can be obtained with multiple scans as shown in Fig. 1(b).The tilt-angle θ of air-table is given by

$$\theta = \sin^{-1}\left(\frac{L}{R_{\mathrm{bfs}}}\right), \tag{1}$$

where L is the distance between probe tip and rotation axis of air-table and R_{bfs} is the radius of curvature of BFS.

The surface result is given by $\Delta S = S_t - S_0$, where S_t is the probe reading and S_0 is the ideal aspherical departure from the BFS.

2.2 *Model Setup*

An SAP has three components: mirror (on turntable), probe, and air-table, which carries the probe. As shown in Fig. 1(a), the rotation axis of the turntable coincides with the center of BFS; the air-table is tilted and its rotation axis goes through the center of BFS; the probe is aligned at the end of the arm and its detect direction points to C_{bfs} so that the probe would measure the aspheric departure from BFS. The error sources of the components are listed in Table 1. In this section, the test result of SAP for axisymmetric asphere will be described in a geometry model, and the analytic solution will be explained.

Table 1 Alignment requirement of SAP.

Items	Alignment goal	Error source
Mirror	Center of mirror coincide with the rotation axis of turntable	Decentration
Air-table	Rotation axis of air-table turntable goes through C_{bfs}	Tilt, decentration
Probe	Detect direction points to C_{bfs}	Tilt
	Coincides with the geometric center of mirror at null position[a]	Decentration

[a]Null position: probe point to the center of mirror as shown in Fig. 1(a).

2.2.1 *Geometry of asphere*

The geometry of points P on axisymmetric optic[1] is shown in Fig. 2, and given by

$$\begin{cases} r^2 - 2Rz + (k+1)z^2 = 0(\text{aspheric-equation}) \\ S\cdot\cos(\xi) + z = R_{\mathrm{bfs}} \\ S\cdot\sin(\xi) = r \end{cases}, \tag{2}$$

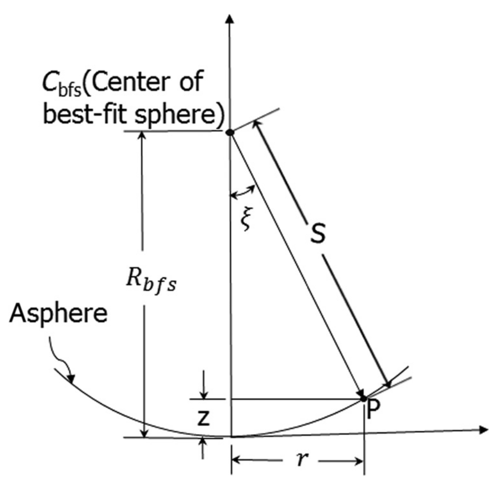

Fig. 2 Distance between surface of axisymmetric asphere and center of BFS.

where r is the distance of point P to optic axis, R is the radius of curvature at vertex, k is the conic constant, and ξ is the angle of elevation of point P.

Based on formulas in Eq. (2), we get the aspheric departure from BFS associated with ξ by

$$S_0 = F(\xi) = R_{\text{bfs}} - S$$
$$= R_{\text{bfs}} - \frac{2RR_{\text{bfs}} - (1+k)R_{\text{bfs}}^2}{K_1 \cos(\xi) + \sqrt{R^2 - K_2 \sin^2(\xi)}}, \tag{3}$$

where $K_1 = R - R_{\text{bfs}}(k+1)$, $K_2 = R_{\text{bfs}}^2(k+1) - 2RR_{\text{bfs}} + R^2$.

2.2.2 *Analytical model of Swing Arm Profilometer*

The coordinate systems and parameters in the SAP model are shown in Fig. 3. Coordinate system $OXYZ$ and $O_2X_2Y_2Z_2$ are both in right-hand coordinate.

The parameters of the SAP system are described below:

$OXYZ$ represents SAP test coordinate system;
$O_2X_2Y_2Z_2$ represents air-table coordinate system;
P' is the point on spherical track of SAP test;
P'' is projection on XY-plane of point P';
β is air-table spin angle;
α is rotate angle of turntable;
ρ is polar radius of test point P';
η' is polar angle of point P''.

The coordinate of points P' in the $OXYZ$ system is expressed by

$$x = R_{\text{bfs}} \cdot \sin(\xi) \cdot \cos(\eta'),$$
$$y = R_{\text{bfs}} \cdot \sin(\xi) \cdot \sin(\eta'),$$
$$z = R_{\text{bfs}} - R_{\text{bfs}} \cdot \cos(\xi). \tag{4}$$

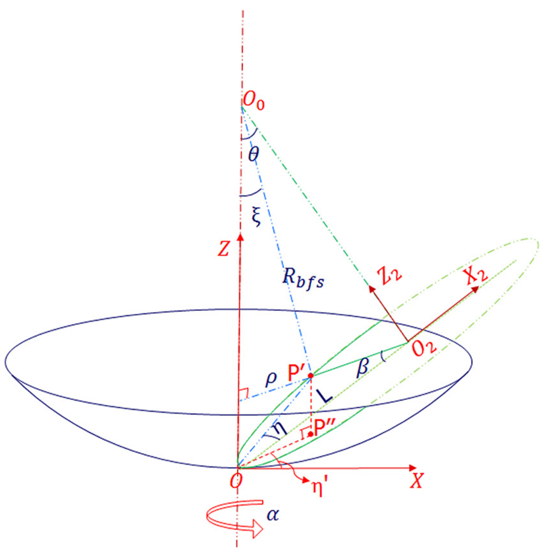

Fig. 3 Parameters of SAP system.

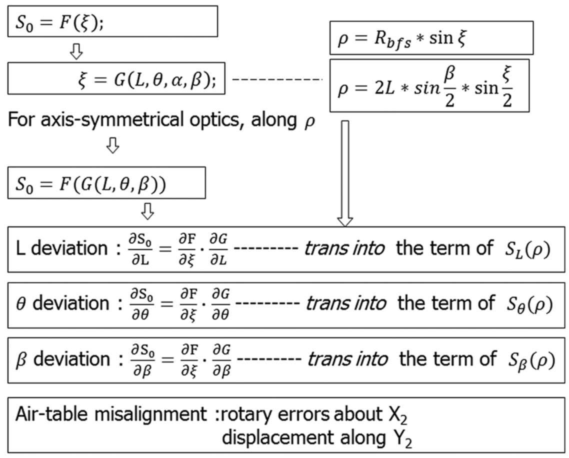

Fig. 4 Flowchart of analytical model.

According to knowledge of triangular geometry, we get

$$\rho = 2\ L \cdot \sin\left(\frac{\beta}{2}\right) \cdot \cos\left(\frac{\pi - \xi}{2}\right), \tag{5}$$

$$\xi = G(L, \beta, R_{\text{bfs}}) = 2\sin^{-1}\left(\frac{L \cdot \sin(\beta/2)}{R_{\text{bfs}}}\right); \qquad \beta \in (0, 2\pi), \tag{6}$$

$$\eta = \tan^{-1}\left(\frac{L \cdot \sin(\beta)}{L \cdot [1 - \cos(\beta)] \cdot \cos(\theta)}\right). \tag{7}$$

As the mirror turntable rotated angle α, we get $\eta' = \eta + \alpha$. In the SAP test system, the relationship between test results and parameters of SAP could be built through Eqs. (3), (6), and (7). Based on this, misalignment problems are discussed in detail in Sec. 2.3, and explicit solutions are derived by performing partial derivative and series expansion, as the flowchart of process shown in Fig. 4.

2.3 *Misalignment Analysis*

2.3.1 *Mirror misalignment error*

In a spherical coordinate system, coordinate of points P on a mirror as shown in Fig. 2 is given by

$$x = r \cdot \cos(\psi); \qquad y = r \cdot \sin(\psi), \tag{8}$$

where r is the polar radius and ψ is the polar angle in XY-plane. According to the knowledge of perfect differential, we get

$$\mathrm{d}r = \cos(\psi)\mathrm{d}x + \sin(\psi)\mathrm{d}y;$$
$$\mathrm{d}\psi = -\frac{\sin(\psi)}{r}\mathrm{d}x + \frac{\cos(\psi)}{r}\mathrm{d}y. \tag{9}$$

The axisymmetric optical surface is represented by

$$z = \frac{r^2}{R\left[1 + \sqrt{1 - (k+1)\frac{r^2}{R^2}}\right]}. \tag{10}$$

Meanwhile, by performing series expansion, the departure toward C_{bfs} is represented by

$$S_0 = R_{\mathrm{bfs}} - \sqrt{x^2 + y^2 + (z - R_{\mathrm{bfs}})^2} = c_1 r^2 + c_2 r^4 + o(r^4), \tag{11}$$

where

$$c_1 = -\frac{R - R_{\mathrm{bfs}}}{2RR_{\mathrm{bfs}}};$$
$$c_2 = -\frac{R - R_{\mathrm{bfs}}}{R_{\mathrm{bfs}}} \cdot \frac{1+k}{8R^3} + \left[\frac{(R - R_{\mathrm{bfs}})^2}{R_{\mathrm{bfs}}^3} + \frac{k}{R_{\mathrm{bfs}}}\right]\frac{1}{8R^2},$$

$o(r^4)$ is fourth minimum order of r.

The effect of mirror decentration is obtained according to

$$\frac{\partial S_0}{\partial x} = \frac{\partial S_0}{\partial r} \cdot \frac{\partial r}{\partial x} = (2c_1 r + 4c_2 r^3)\cos(\psi) + o(r^3),$$
$$\frac{\partial S_0}{\partial y} = \frac{\partial S_0}{\partial r} \cdot \frac{\partial r}{\partial y} = (2c_1 r + 4c_2 r^3)\sin(\psi) + o(r^3). \tag{12}$$

It is known from Eq. (12) that deviation of the axisymmetric mirror in X-axis and Y-axis result in 0 and 90 deg coma, respectively.

For a real parabolic mirror, whose $k = -1$, $D = 2000$ mm, $R = 6000$ mm, $R_{\mathrm{bfs}} = 6100$ mm, its deviation in X-axis direction is 1 mm. Ignore tilt, and normalize r by $r_{\max} = D/2$, we get the system error allocated to coma terms expressed as $[r(-2 + 3r^2) \cdot \cos\psi]$ by

$$Z_{\mathrm{coma}} = \frac{4c_2}{3} r_{\max}^3 \delta x = 7.587 \times 10^{-4} \text{ mm}.$$

It means that per 1 mm decentration of 2-m diameter polibolid along X-axis produces coma in 1.5 μm PV and 0.27 μm RMS.

2.3.2 *Arm L deviation*

In the SAP system, by performing Taylor expansion, $S(\xi)$ in Eq. (3) can be represented by

$$S_0(\xi) = a_1\xi^2 + a_2\xi^4 + a_3\xi^6 + o(\xi^6), \tag{13}$$

where

$$a_1 = \frac{(K_1 + K_2/R)R_{\mathrm{bfs}}}{2(K_1 + R)};$$
$$a_2 = \left[-\frac{(-K_1 - K_2/R)^2}{4(K_1 + R)^2} + \frac{K_1 - 3K_2^2/R^3 + 4K_2/R}{24(K_1 + R)}\right] \cdot R_{\mathrm{bfs}}.$$

On the other hand, by eliminating ξ from Eqs. (5) and (6), the relationship between β and ρ is obtained as

$$\left[L \cdot \sin\left(\frac{\beta}{2}\right)\right]^2 = \frac{R_{\mathrm{bfs}}}{2}\left(R_{\mathrm{bfs}} - \sqrt{R_{\mathrm{bfs}}^2 - \rho^2}\right). \tag{14}$$

With substitution for β from Eq. (14), the differential relationship between ξ and L according to Eq. (6) is given by

$$\frac{\partial \xi}{\partial L} = \frac{2\sin(\beta/2)}{\sqrt{R_{\mathrm{bfs}}^2 - L^2\sin^2(\beta/2)}} = \frac{2}{L\left(R_{\mathrm{bfs}} + \sqrt{R_{\mathrm{bfs}}^2 - \rho^2}\right)}. \tag{15}$$

With $\xi = \sin^{-1}(\rho/R_{\mathrm{bfs}})$ and by performing Taylor expansion, we get partial derivative about ρ according to

$$\frac{\partial S_0}{\partial L} = \frac{\partial F}{\partial \xi} \cdot \frac{\partial \xi}{\partial L} = [2a_1\xi + 4a_2\xi^3 + 6a_3\xi^5 + o(\xi^5)] \cdot \frac{2}{L\left(R_{\mathrm{bfs}} + \sqrt{R_{\mathrm{bfs}}^2 - \rho^2}\right)},$$
$$\frac{\partial S_0}{\partial L} = b_1\rho^2 + b_2\rho^4 + o(\rho^4), \tag{16}$$

where

$$b_1 = \frac{2a_1}{L \cdot R_{\mathrm{bfs}}^2}; \qquad b_2 = \frac{5a_1 + 24a_2}{6\,L \cdot R_{\mathrm{bfs}}^4}.$$

For axisymmetric mirror, from Eq. (16), it is known that deviation of L results in defocus and spherical errors. For a 2-m diameter parabolic mirror, $L = 500$ mm, $\delta L = 1$ mm; normalizing ρ by half diameter of mirror, which is 1000 mm, we get

$$\Delta S_L = \frac{\partial S_0}{\partial L} \cdot \delta L = -0.786 \times 10^{-3}(1 - 6\rho^2 + 6\rho^4) - 5.93 \times 10^{-2}\rho^2 + 0.786 \times 10^{-3}; \quad \text{here, } \rho \in [0,1]. \tag{17}$$

With respect to the normalized Zernike terms of SA_3 (primary spherical aberration), expressed as $(1 - 6\rho^2 + 6\rho^4)$, the value of SA_3 in ΔS_L is -0.786 μm.

It means that L deviation per 1 mm results in SA_3 error of 1.179 μm in PV, which is 1.5 times the value of SA_3. Here, a simulation is presented. We first tested the 2-m diameter parabolic mirror by SAP as the result shown in Fig. 5(a). Then, 1-mm deviation is joined into L during data processing and the test result is shown in Fig. 5(b). Difference between two maps is 1.184 μm in PV and 0.267 μm in RMS as shown in Fig. 5(c). The simulated result of 1.184 μm differs 0.4% from calculated result of 1.179 μm which is negligible and verified each other.

2.3.3 *Tilt-angle θ deviation*

According to Eq. (1), we get

$$\Delta S_\theta = \frac{\partial S_0}{\partial \theta} \cdot \delta\theta = \frac{\partial S_0}{\partial L} \cdot R_{\mathrm{bfs}} \cdot \cos(\theta) \cdot \delta\theta. \tag{18}$$

It means that the influence from tilt-angle deviation has the same form with the one from Arm L errors with a factor of $R_{\mathrm{bfs}}\cos\theta$. In the example above, per 1-mm deviation of L equals to about 0.01 deg deviation of θ.

2.3.4 *Rotation error $\delta\beta$ of air-table*

As presented in Table 1, the probe should be aligned to coincide with the center of mirror at null position shown

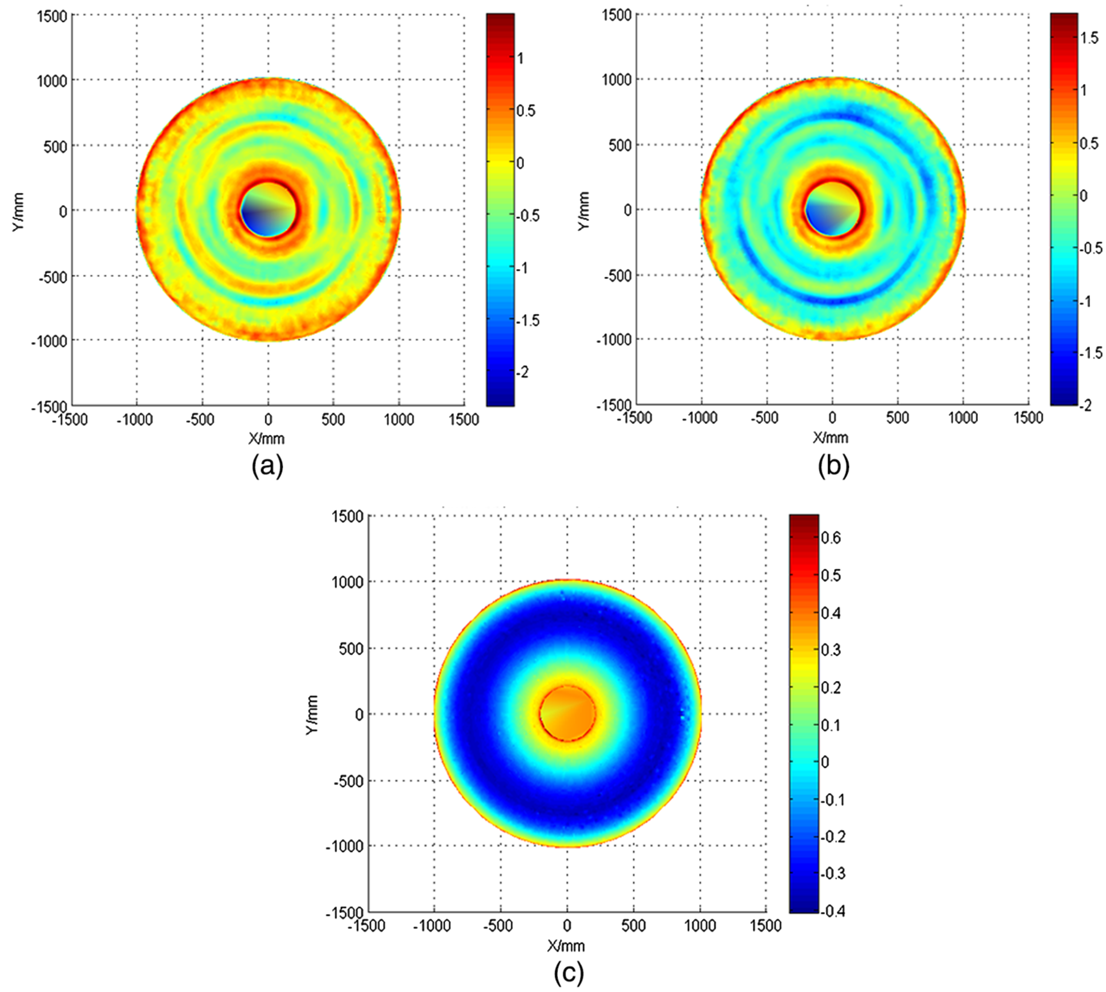

Fig. 5 Simulation of *L* deviation: (a) initial SAP test result PV $= 3.743\ \mu$m, RMS $= 0.45\ \mu$m; (b) SAP test result with *L* deviated 1 mm PV $= 3.724\ \mu$m, RMS $= 0.605\ \mu$m; (c) difference PV $= 1.184\ \mu$m, RMS $= 0.267\ \mu$m.

in Fig. 1(a). The length of the arm is adjusted to assure the alignment in X-axis direction, and the spin angle β is adjusted to assure the alignment in Y-axis direction. So the decentration in Y-axis direction of probe means a constant delayed or advanced error of angle β. For axisymmetric optics, the terms of air-table errors in different angle α are the same. For easy description, we discuss the case in single scan, where $\alpha = 0$ deg. According to Eq. (6), we get the partial derivative of β by

$$\frac{\partial \xi}{\partial \beta} = \frac{L\cos(\beta/2)}{\sqrt{R_{\mathrm{bfs}}^2 - L^2\sin^2(\beta/2)}}. \tag{19}$$

So according to Eq. (3), we obtain

$$\frac{\partial S_0}{\partial \beta} = \frac{\partial F}{\partial \xi}\cdot\frac{\partial \xi}{\partial \beta} = -\frac{2RR_{\mathrm{bfs}} - (1+k)R_{\mathrm{bfs}}^2}{[K_1\cos(\xi) + \sqrt{R^2 - K_2\sin^2(\xi)}]^2} \cdot \left[K_1\sin(\xi) + \frac{K_2\sin(2\xi)}{2\sqrt{R^2 - K_2\sin^2(\xi)}}\right] \cdot \frac{L\cos(\beta/2)}{\sqrt{R_{\mathrm{bfs}}^2 - L^2\sin^2(\beta/2)}}. \tag{20}$$

For the parabolic mirror, as alignment accuracy of probe along Y-axis direction $\delta y = 1$ mm, which means $\delta\beta \approx \delta y/L = 2$ mrad, the errors on single scan line with tilt removed are shown in Fig. 6(a). By rotating single scan around axis of mirror turntable, errors in the whole surface are given. Due to noncoincidence at crossings of neighboring scan lines, fitting effect on the surface is in the form of random noise as shown in Fig. 6(b) with 0.2 μm in PV and 0.01 μm in RMS.

2.3.5 *Air-table misalignment errors*

Approximation of swing arm profilometer test. In the coordinate system $O_2X_2Y_2Z_2$ as shown in Fig. 3, the misalignment errors of air-table mainly include displacements along X_2-axis and Y_2-axis direction, and rotary deviations about X_2-axis and Y_2-axis.

As a matter of fact, air-table displacement along X_2-axis is equivalent to the deviation of parameter L, and air-table rotary deviation about Y_2-axis is equivalent to the deviation of parameter θ of SAP system, which resulted in defocus and aspherical aberrations. Air-table displacement along Y_2-axis and rotary deviation about X_2-axis deflect the rotary axis of

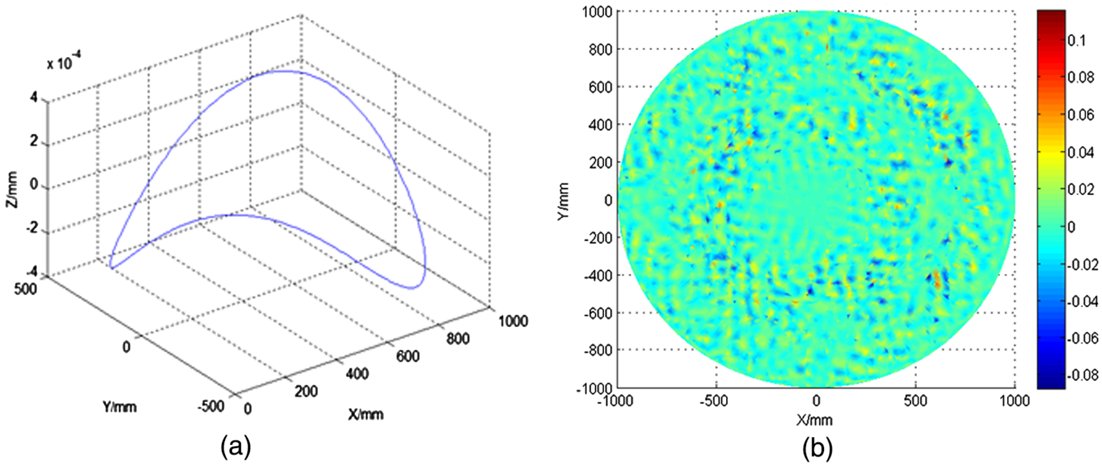

Fig. 6 Errors result from β deviation: (a) error result in single scan data with tilt removed and (b) error result in whole surface.

air-table from rotary axis of mirror turntable, which is mainly discussed later.

In the SAP test model, substituting for $\xi = \sin^{-1}(\rho/R_{\mathrm{bfs}})$, the aspherical departure in Eq. (3) becomes

$$\Delta S_0 = R_{\mathrm{bfs}} - \frac{2RR_{\mathrm{bfs}} - (1+k)R_{\mathrm{bfs}}^2}{K_1\sqrt{1-\rho^2/R_{\mathrm{bfs}}^2} + \sqrt{R^2 - K_2\rho^2/R_{\mathrm{bfs}}^2}}. \tag{21}$$

The approximate aspherical departure is used in some cases[8,10] as given by

$$S_{\mathrm{appr}} = R_{\mathrm{bfs}} - \sqrt{\rho^2 + [z(\rho) - R_{\mathrm{bfs}}]^2}, \tag{22}$$

where

$$z = \frac{\rho^2}{R(1+\sqrt{1-(k+1)\rho^2/R^2})}.$$

Approximation error is given in the example of 2-m diameter parabolic mirror. The exact aspherical departure is 142.385 μm in PV as shown in Fig. 7(a) and the approximate one is 142.443 μm in PV as shown in Fig. 7(a). The difference between exact solution and approximate one is about 49 nm in PV and 0.017 μm in RMS with defocus removed as shown in Fig. 7(c). Since the approximate error is acceptable, the simplified expression of aspheric departure in Eq. (22) will be used in the work below.

Air-table rotatory errors about $\boldsymbol{X}_2$*-axis.* In the SAP model shown in Fig. 3, after air-table rotated a tiny angle u about X_2, the coordinate (x, y, z) of points P on the single scan line $(\alpha = 0)$ turns out to be (x', y', z') as follows:

$$\begin{pmatrix} x' \\ y' \\ z' \end{pmatrix} = r_y' \cdot r_{x(u)} \cdot r_y \cdot \begin{pmatrix} x \\ y \\ z \end{pmatrix}, \tag{23}$$

where

$$r_y = \begin{pmatrix} \cos(\theta) & 0 & \sin(\theta) \\ 0 & 1 & 0 \\ -\sin(\theta) & 0 & \cos(\theta) \end{pmatrix},$$

$$r_y' = \begin{pmatrix} \cos(-\theta) & 0 & \sin(-\theta) \\ 0 & 1 & 0 \\ -\sin(-\theta) & 0 & \cos(-\theta) \end{pmatrix},$$

$$r_{x(u)} = \begin{pmatrix} 1 & 0 & 0 \\ 0 & \cos(u) & -\sin(u) \\ 0 & \sin(u) & \cos(u) \end{pmatrix}$$

As u is a minuteness, we obtain

$$\begin{pmatrix} x' \\ y' \\ z' \end{pmatrix} \cong \begin{pmatrix} x - u \cdot y \cdot \sin\theta \\ y - z \cdot \cos\theta \cdot \sin u + x \cdot \sin\theta \cdot \sin u \\ z + u \cdot y \cdot \cos\theta \end{pmatrix}. \tag{24}$$

Meanwhile, center of SAP sphere changed from $(0, 0, R_{\mathrm{bfs}})$ to $(0, \delta y, R_{\mathrm{bfs}})$, where $\delta y = -uR_{\mathrm{bfs}}\cos(\theta)$, then the aspheric departure tested by SAP in a single scan line becomes

$$\begin{aligned} S' &= f(x, y, u) \\ &= R_{\mathrm{bfs}} - \sqrt{x'^2 + (y' - \delta y)^2 + [z(x', y') - R_{\mathrm{bfs}}]^2} \\ &\approx s'(u=0) + \frac{\partial S'}{\partial u} \cdot u. \end{aligned} \tag{25}$$

According to Eq. (22) and Eq. (9), where ρ' here means the polar radius r there, by performing partial derivative, we obtain

$$\begin{aligned} \left.\frac{\partial z(x', y')'}{\partial u}\right|_{u=0} &= \frac{\partial z}{\partial \rho'}\left.\left(\frac{\partial \rho'}{\partial x'} \cdot \frac{\partial x'}{\partial u} + \frac{\partial \rho'}{\partial y'} \cdot \frac{\partial y'}{\partial u}\right)\right|_{u=0} \\ &= \frac{-\rho z \cos(\theta)}{\sqrt{R^2 - (1+k)\rho^2}}. \end{aligned} \tag{26}$$

Here,

$$z = R_{\mathrm{bfs}} - \sqrt{R_{\mathrm{bfs}}^2 - \rho^2}.$$

The analytical solution of the test error from air-table rotatory deviation about X_2-axis is given by

$$S_u = \frac{\partial S'}{\partial u}\bigg|_{u=0} \cdot u = \frac{xy \sin\theta - y(x\sin\theta - \sqrt{R_{\mathrm{bfs}}^2 - \rho^2}\cos\theta + R_{\mathrm{bfs}}\cos\theta) + [z(\rho) - R_{\mathrm{bfs}}]\frac{\rho z \cos\theta}{\sqrt{R^2-(1+k)\rho^2}}}{\sqrt{\rho^2 + [z(\rho) - R_{\mathrm{bfs}}]^2}} u. \tag{27}$$

The consequent error of u being 0.01 deg is calculated, as error in a single scan with tilt removed shown in Fig. 8(a). By rotating the single scan around axis of mirror turntable, the effect on the whole surface is mainly in a SA_3 form in 0.43 μm PV and 0.012 μm RMS as shown in Fig. 8(b).

Air-table displacement along $\mathbf{Y}_2$*-axis.* After air-table displaced μ along Y_2-axis, the data transformation matrix is given by

$$\begin{pmatrix} x' \\ y' \\ z' \end{pmatrix} = \begin{pmatrix} x \\ y+\mu \\ z \end{pmatrix}. \tag{28}$$

The tested aspheric departure in Eq. (22) of a single scan line becomes

$$S' = f(x,y,u) = R_{\mathrm{bfs}} - \sqrt{x'^2 + (y' - \delta y)^2 + [z(x',y') - R_{\mathrm{bfs}}]^2}, \tag{29}$$

Here, $\delta y = \mu$. In a similar way explained in part B, we get

$$\frac{\partial z(x',y')'}{\partial u}\bigg|_{u=0} = \frac{y}{\sqrt{R^2-(1+k)\rho^2}}, \tag{30}$$

$$S_\mu = \frac{\partial S'}{\partial \mu}\bigg|_{\mu=0} \cdot \mu = -\frac{z(\rho) - R_{\mathrm{bfs}}}{\sqrt{\rho^2 + [z(\rho) - R_{\mathrm{bfs}}]^2}} \cdot \frac{y}{\sqrt{R^2-(1+k)\rho^2}} \cdot \mu. \tag{31}$$

The consequent errors of μ being 0.01 deg are shown in Fig. 9. Error of single scan data with tilt off is shown in Fig. 9(a); due to fitting effect, influence on the whole surface is in the form of random noise with 0.18 μm in PV and 0.01 μm in RMS as shown in Fig. 9(b).

2.4 *Misalignment Tolerance*

Related to the probe range, probe disvertical from surface will result in a small displacement in X/Y-axis and a small quantity of the second order in probe readout,

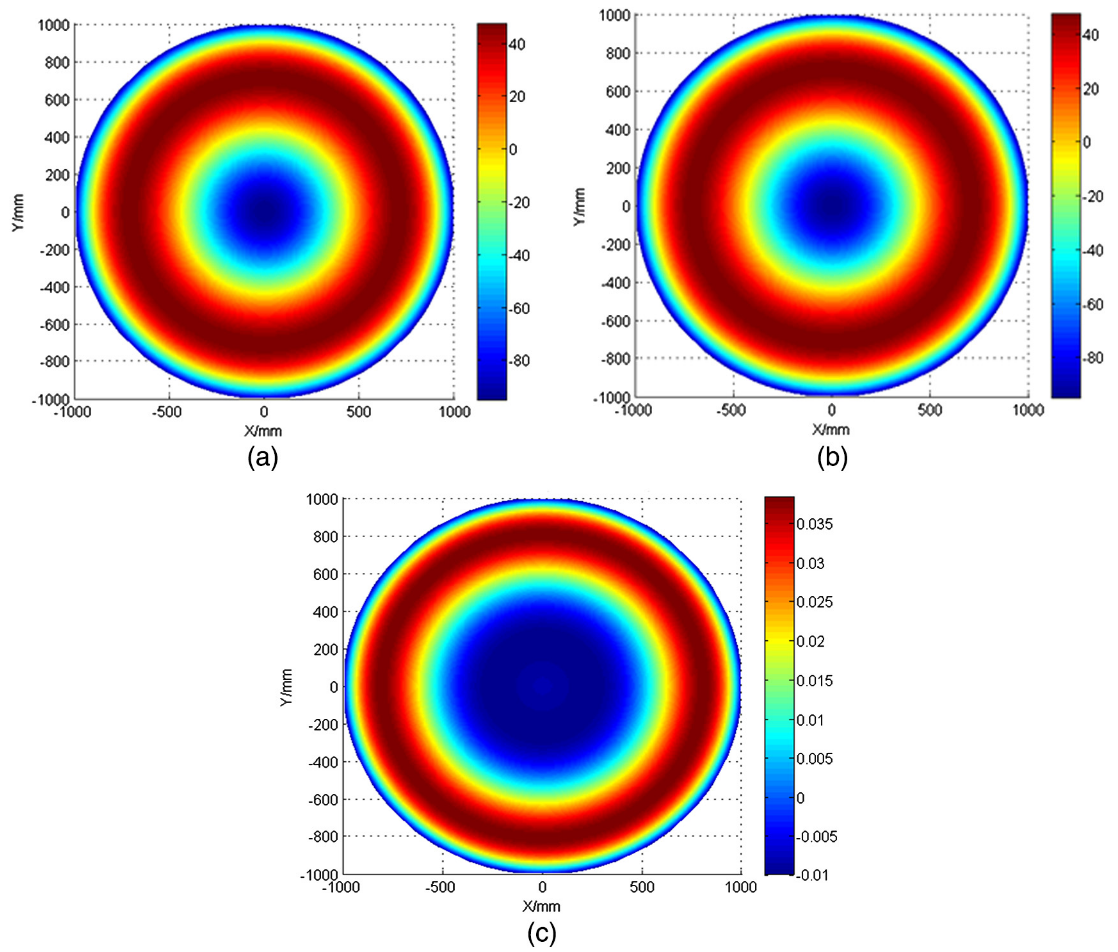

Fig. 7 Comparison of the approximate departure of parabolid from exact one: (a) the exact departure; (b) the approximate departure; and (c) difference.

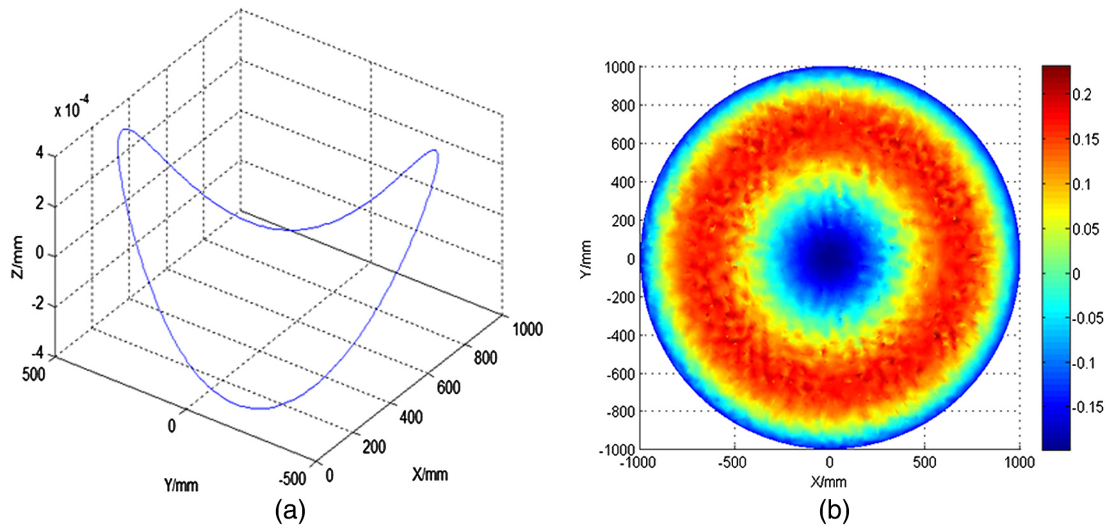

Fig. 8 Influence in test result of air-table with rotary deviation about X_2-axis: (a) errors on single scan data with tilt off and (b) errors on the whole surface.

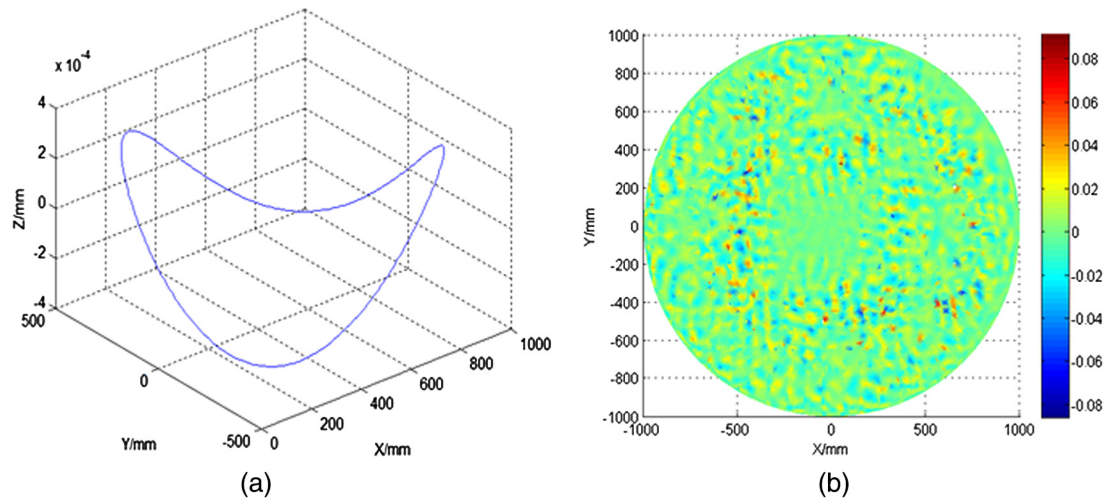

Fig. 9 Influence in test result of air-table displaced along Y_2-axis: (a) errors on single scan data with tilt off and (b) errors on the whole surface.

Table 2 Alignment budget of SAP for 2-m diameter parabolic.

		>5 μm PV, 1 μm RMS		0.5 to 5 μm PV; <1 μm RMS	
Accuracy of surface		Misalignment tolerance	Error in RMS/μm	Misalignment tolerance	Error in RMS/μm
Mirror alignment		1 mm	0.27 (coma)	0.2 mm	0.05 (coma)
Length of arm L		1 mm	0.27 (SA_3)	0.1 mm	0.03 (SA_3)
Tilt-angle θ		0.01 deg	0.27 (SA_3)	0.001 deg	0.03 (SA_3)
Probe alignment	Along arm	0.5 mm	0.14 (SA_3)	0.1 mm	0.03 (SA_3)
	Perpendicular direction of arm[a]	1 mm	0.01 (random)	0.05 mm	0.001 (random)
Air-table posture	Rotate about X_2[b]	0.01 deg	0.12 (SA_3)	0.001 deg	0.012 (SA_3)
	Displaced along Y_2	1 mm	0.01 (random)	0.001 deg	0.001 (random)
Total			0.84		0.11

[a]The misalignment tolerance is related to the length of arm.
[b]The misalignment tolerance is related to R_{bfs}.

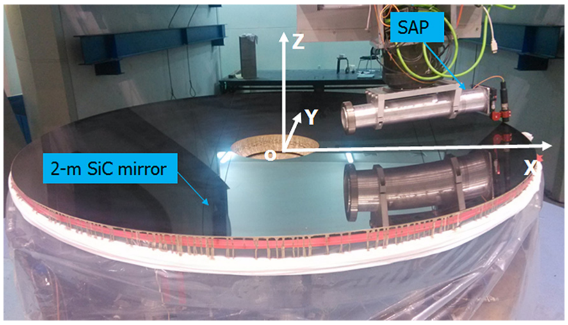

Fig. 10 SAP setup for 2-m diameter paraboloid.

which can be ignored here. From the analyses of the SAP model, the errors from misalignments of SAP for testing axisymmetric surface are in the form of SA_3 and random noise.

It is an expensive and hard work to achieve strict alignment budget. During the rough grinding process, loose alignment is acceptable and more efficient; whereas strict budget is necessary for a higher accuracy surface test. In two phases of different accuracy of surface, misalignment tolerances of SAP for 2-m diameter parabolic are allocated as shown in Table 2.

3 Experiments on 2-m Diameter Parabolic Mirror

In these parts, a particular SAP[14,16] is used to test the 2-m diameter parabolic mirror as an experiment. As SAP setup shown in Fig. 10, the air-table is fixed on the spindle of a grinding/polishing machine, and 2-m diameter mirror is placed on the turntable of the machine. The spindle is used to generate the tilt-angle θ of SAP, and XYZ slide axes are used to adjust the position of SAP.

3.1 *Experiment Verification of Misalignment Analysis*

Due to space limitation, here, we just perform an experiment of air-table displacement along X-axis to verify the analytical model. As explained in Sec. 2.3.5.1, air-table displacement along X-axis is equivalent to the displacement of arm length L. In this experiment, air-table is displaced 2 mm along $+X$-axis to test the misalignment sensitivity of SAP. The influence of displacement in test results is shown in Fig. 11. The initial test result of SAP is shown in Fig. 11(a); the test result after displacement is shown in Fig. 11(b); and their difference is SA_3 errors in 2.325 μm PV as shown in Fig. 11(c). As described in Sec. 2.3.2, per 1 mm L displacement produces 1.179 μm PV SA_3 errors. So the percentage error of experiment results from the calculated solution is 1.4%, which is acceptable. The analytical model is checked as the result coinciding with analytical solution.

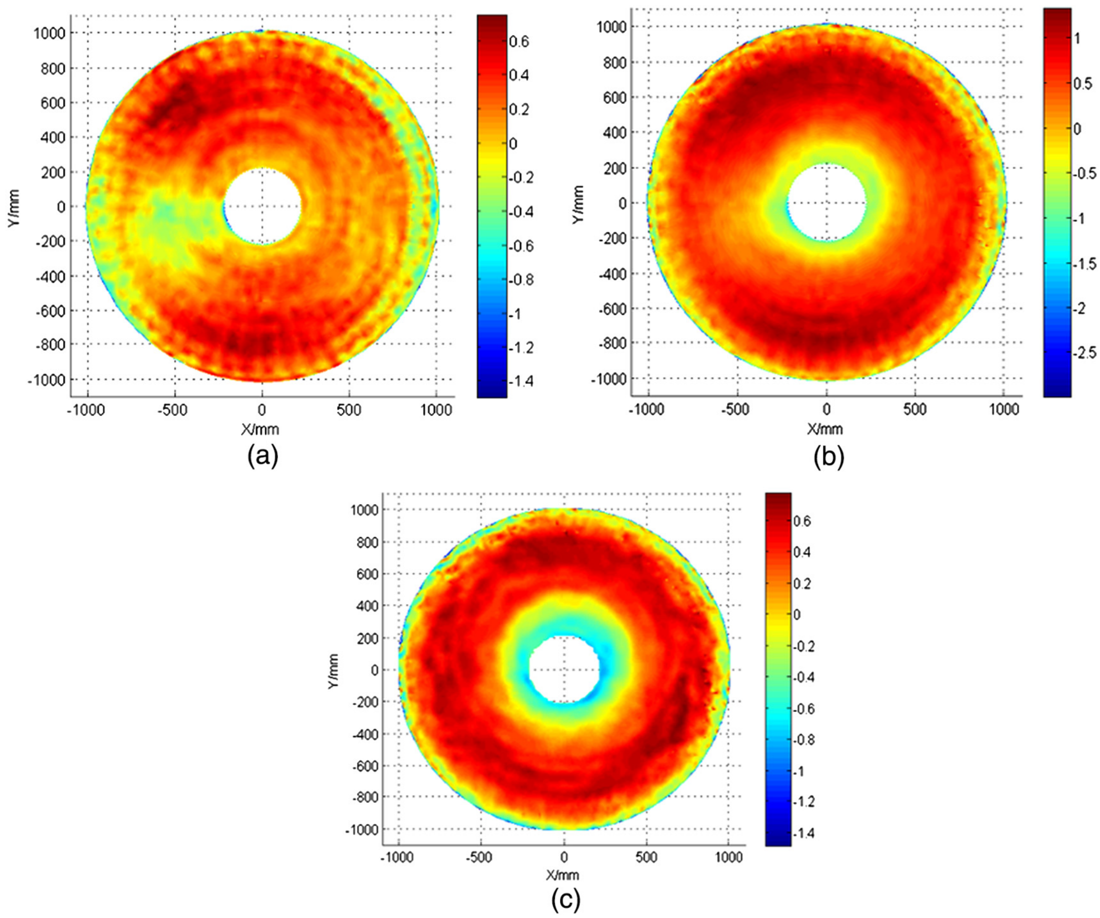

Fig. 11 Influence in test result of air-table displaced along X-axis: (a) before displacement, PV $= 2.247$ μm, RMS $= 0.352$ μm; (b) after displacement, PV $= 4.324$ μm, RMS $= 0.774$ μm; and (c) difference, PV $= 2.325$ μm, RMS $= 0.364$ μm.

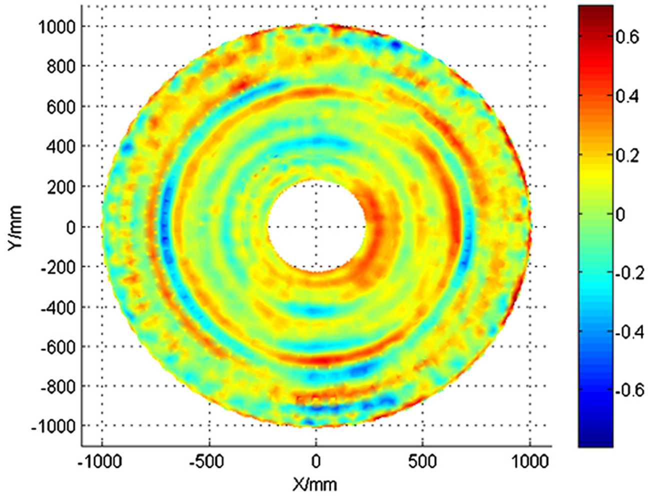

Fig. 12 SAP test result for 2-m diameter mirror, PV = 1.495 μm, RMS = 0.166 μm.

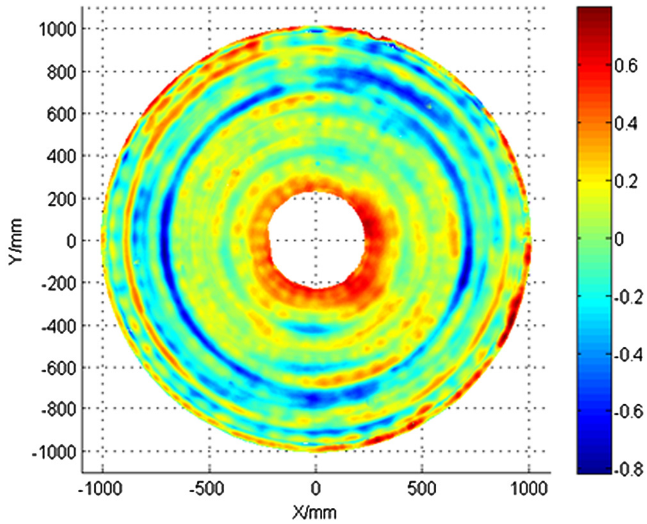

Fig. 13 Interferometer test result for 2-m diameter mirror, PV = 1.618 μm, RMS = 0.226 μm.

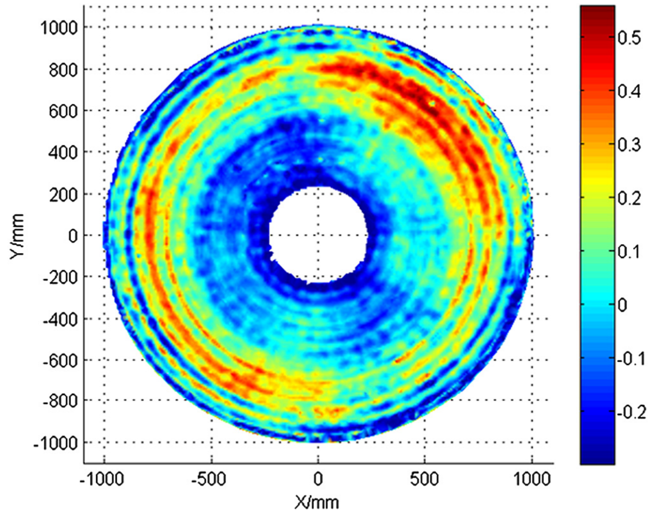

Fig. 14 The difference between SAP and Interferometer test result, PV = 0.857 μm, RMS = 0.167 μm.

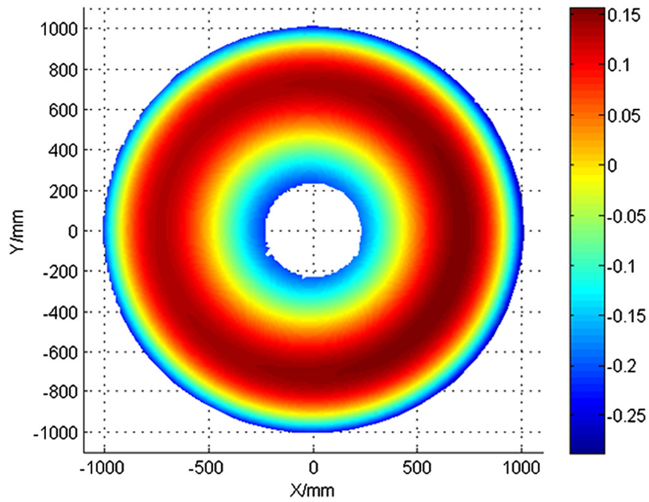

Fig. 15 Coma and SA_3 terms in the difference between SAP and interferometer test, PV = 0.444 μm, RMS = 0.108 μm.

3.2 *Verified with Interferometer Test*

The interferometer is mounted above the mirror in the test tower. To verify the test accuracy of SAP, the mirror is polished and is measured by the interferometer in the same posture. SAP setup is calibrated according to the tolerance given in Table 2, and the test result is 1.495 μm in PV, 0.166 μm in RMS as shown in Fig. 12. The interferometer test result is 1.618 μm in PV and 0.226 μm in RMS as shown in Fig. 13. A direct subtraction between the SAP test result and the interferometer test result without any low-order terms removed expect power shows the difference of ~0.857 μm in PV and 0.167 μm in RMS as shown in Fig. 14.

As analyzed in Sec. 2, misalignments of SAP for testing axisymmetric surfaces mainly produce coma and SA_3 errors. Here, as shown in Fig. 15, the coma and SA_3 errors in the deviation between SAP and the interferometer test result are 0.444 μm PV and 0.108 μm RMS within the limits of error budget 0.11 μm RMS given in Table 2. The experiment result verified the error budget well. It means that according to the error budget, we achieve the SAP test for low-order errors with accuracy of 0.1 μm RMS. Due to the different sampling density, some high-frequency details in Figs. 13 and 14 do not match well. Other unexpected middle and high-frequency errors are caused by errors such as sensor probe read error and air-table and mirror turntable vibration errors.

4 Conclusion

The misalignment errors of SAP have been discussed in detail and analytical solutions are derived. The sensitivity ratios of misalignment for testing a 2-m diameter paraboloid are calculated: per L deviation of 1 mm brings SA_3 in 1.2 μm PV, and 0.01 deg tilt-error of air-table around X_2 brings mainly SA_3 error in 0.4 μm PV; while 1-mm displacement of air-table along Y_2 and 0.1 deg delay of air-table rotary angle both lead to random error of 0.2 μm in PV. Alignment tolerance is allocated to assure the test accuracy and verified experiments for the model are carried out. According to the error budget, we achieve the SAP test for low-order errors with accuracy of 0.1 μm RMS. Compared with the interferometer test result, the accuracy of the SAP test on a 2-m diameter mirror is 0.9 μm in PV and 0.2 μm in RMS (only power term removed). Further work will focus on calibration of the middle and high-frequency errors to improve the test accuracy.

Acknowledgments

This work was supported by the National Natural Science Foundation of China (61036015 and 61210015) and the National High Technology Research & Development Program of China (O8663NJ090).

References

1. D. S. Anderson, R. E. Parks, and T. Shao, "A versatile profilometer for aspheric optics," in *Proc. of OF&T Workshop Technical Digest*, Vol. **11**, pp. 119–122, Academic, Monterey, California (1990).
2. D. S. Anderson and J. H. Burge, "Swing-arm profilometry of aspherics," *Proc. SPIE* **2536**, 169–179 (1995).
3. P. Su et al., "Swing arm optical CMM for aspherics," *Proc. SPIE* **7426**, 74260J (2009).
4. J. H. Burge, "Fabrication and testing of 1.4-m convex off-axis aspheric optical surfaces," *Proc. SPIE* **7426**, 74260L (2009).
5. P. Su et al., "Swing arm optical CMM: self calibration with dual probe shear test," *Proc. SPIE* **8126**, 81260W (2011).
6. P. Su, "Swing-arm optical coordinate measuring machine: modal estimation of systematic errors from dual probe shear measurements," *Opt. Eng.* **51**(4), 043604 (2012).
7. Y. Wang et al., "Swing arm optical coordinate-measuring machine: high precision measuring ground aspheric surfaces using a laser triangulation probe," *Opt. Eng.* **51**(7), 073606 (2012).
8. L. C. Perelman, J. Paradis, and E. Barrett, *Mayfield Handbook of Technical and Scientific Writing*, Mayfield, Mountain View, California (1997).
9. A. Lewis et al., "Accurate arm profilometry traceable metrology for large mirrors," in *Proc. Simp. de Metrología*, pp. 101–105, Academic, Mexico, (2006).
10. H. Jing et al., "Development and experimental validation of a versatile prototype swing arm profilometer for measuring optical surface," *J. Eur. Opt. Soc.-Rapid Publ.* **6**, 11052 (2011).
11. H. Jing et al., "Measurement of an off-axis parabolic mirror using coordinates measurement machine and swing arm profilometer during the grinding process," *Proc. SPIE* **8415**, 84150K (2012).
12. I. K. Sung et al., "A swing arm method for profile measurement of large optical concave surfaces in the lapping process," *Int. J. Adv. Manuf. Technol.* **29**, 113–117 (2006).
13. L. Jia, "Principle and experiments of swing-arm profilometer," *Opt. Precision Eng.* **15**(4), 499–504 (2007).
14. L. Xiong et al., "Measurement of 2m SiC aspheric mirror based on swing arm profilometer," *Acta Opt. Sin.* **35**(12), 1212002 (2015).
15. L. Chen et al., "Research on the measurement technology of effective arm length of swing arm profilometer," *Proc. SPIE* **9280**, 92800P (2014).
16. X. Luo, "Swing arm profilometer: improving the testing accuracy of large mirrors with shorter arms," *Chin. Opt. Lett.* **12**, S22202 (2014).
17. X. Luo, *Fabrication of Large Aspheric Using Stressed Lap with Orbital Tool Motion*, pp. 67–86, Changchun Institute of Optics, Fine Mechanics and Physics, Chinese Academy of Sciences, Changchun (2011).

Ling Xiong received her BS degree in optics from the Northwestern Polytechnical University in 2012. She is currently a PhD student at Changchun Institute of Optics, Fine Mechanics and Physics, Chinese Academy of Sciences (CIOMP). She is working on optical testing for large diameter optic segments. Her research interests include swing arm profilometer testing.

Xiao Luo received his BA degree in precision machinery and precision instrumentation in 2006 from the University of Science and Technology of China and a PhD in optical engineering in 2011 from CIOMP. His is an associate professor at CIOMP. His work includes fabrication with stressed lap and testing with swing arm profilometer for large aspherics. His interests also include hydraulic polishing support of large mirrors and MRF processing of large mirrors.

Zhenyu Liu received his BS degree in physics in 2008 from Jilin University and a PhD in optical engineering in 2013 from CIOMP. His current position is research assistant at CIOMP. His research interest is optical fabricating technology for large aspheric SiC mirror.

Xiaokun Wang received his BS degree from Jiangsu Normal University in 2003 and a PhD from CIOMP. He is currently a professor and PhD adviser at CIOMP. His research focuses on fabricating and testing for large aspheric optics, especially on technology of subaperture stitching interferometry.

Haixiang Hu received his BS degree in physics in 2012 from the University of Science and Technology of China. He is currently a PhD student at CIOMP. His research interest includes high-efficiency processing and testing technology for large mirrors.

Feng Zhang received his BS and MS degrees from Changchun University of Science and Technology and a PhD from CIOMP. He is a professor and PhD adviser at CIOMP. His research focuses on advanced technologies for optical fabrication.

Ligong Zheng received his BA degree in mechanical design and manufacturing from Jilin University of Technology in 1992 and a PhD in optical engineering from CIOMP. He is a professor at CIOMP. His research focuses on advanced technologies for optical fabrication and testing.

Xuejun Zhang received his BA degree from Jilin University of Technology in 1992, MS and PhD degrees from CIOMP. He is a professor and PhD adviser at CIOMP, where he is also director of the Key Laboratory of Optical System Advanced Manufacturing Technology. His research interest is advanced optical system manufacture.